Materials Research Express

PAPER • **OPEN ACCESS**

Structural relaxation probed by resistance drift in amorphous germanium

To cite this article: Ning-Ning Dong *et al* 2020 *Mater. Res. Express* **7** 036410

View the article online for updates and enhancements.

This content was downloaded from IP address 202.198.37.133 on 08/04/2021 at 15:21

Materials Research Express

PAPER

Structural relaxation probed by resistance drift in amorphous germanium

Ning-Ning Dong[1,2], Jian-Gen Xu[1], Jin-Jiang Cui[1,4] and Xiaodong Wang[3,4]

[1] Suzhou Institute of Biomedical Engineering and Technology, Chinese Academy of Sciences, Suzhou 215163, People's Republic of China
[2] Academy for Engineering & Technology, Fudan University, Shanghai 200433, People's Republic of China
[3] Changchun Institute of Optics, Fine Mechanics and Physics, Chinese Academy of Sciences, Changchun 130033, People's Republic of China
[4] Authors to whom any correspondence should be addressed.

E-mail: cuijj@sibet.ac.cn **and** wangxiaodong@ciomp.ac.cn

Keywords: structural relaxation, amorphous germanium, MRO, CRN

OPEN ACCESS

RECEIVED
12 December 2019

REVISED
10 March 2020

ACCEPTED FOR PUBLICATION
17 March 2020

PUBLISHED
30 March 2020

Original content from this work may be used under the terms of the Creative Commons Attribution 4.0 licence.

Any further distribution of this work must maintain attribution to the author(s) and the title of the work, journal citation and DOI.

Abstract

Amorphous germanium films with different thicknesses are deposited by magnetron sputtering (MS) method. Optical band gap and surface resistance are characterized. Our analysis reveals that there are three kinds of structural relaxation (SR) that may occur in amorphous germanium (a-Ge), and they are spontaneous SR (SSR), annealing-induced SR (AISR), and medium range order (MRO)-to-continuous random network (CRN) Sr Samples all demonstrate a band gap widening after these kinds of Sr The properties and mechanisms of SSR, AISR, and MRO-to-CRN SR are elucidated, respectively, which sheds some light on the controversies about SR in a-Ge films. In addition, some experimental results about SSR and AISR are also provided.

1. Introduction

Structural transformation of amorphous tetrahedral semiconductor has attracted much interest among researchers [1–4], and SR is one of hot topics [4–13]. Theye group [4] found that SR of a-Ge includes SSR after deposition and AISR, and the conductivity decreases with the increment of time (SSR) and temperature (AISR). Since then, scientists referred to AISR as SR, and many experimental and theoretical literatures about AISR of a-Si and a-Ge were published [5–15]. Roorda group [6–11] made great efforts to elucidate mechanisms of AISR, and they proposed a compelling scenario for SR of amorphous silicon (a-Si) and a-Ge that encompasses both defect removal and a reduction in average bond-angle distortion based on high energy X-ray diffraction measurements [11]. The observation of high volume of MRO in a-Si and a-Ge [12–14] complicated SR [15–17] although the existent of MRO in a-Si and a-Ge is still in debate [18, 19]. Cheng *et al* [16] provided an experimental evidence of a diminishing of MRO in ion-implanted a-Si resulting from thermal annealing based on analysis of fluctuation electron microscopy measurement, and they believed that there is a strong correlation between structure disordering and thermal relaxation. Subsequently, Roorda [17] questioned Cheng's opinion, and argued that structure disordering and thermal relaxation are essentially unrelated two processes. In 2016, Okugawa studied SR in a-Ge films by aging at ambient temperature [20], and crystallization of a-Ge by electron irradiation [21], and thermal annealing [22]. They argued that a small fraction of metastable MRO clusters exist in as-deposited samples, and there is a reduction of MRO due to aging at ambient temperature, electron irradiation, and thermal annealing, respectively. Their arguments are in line with the views of Cheng. In 2020, Özyilmaz group prepared free-standing monolayer amorphous carbon, and it was found that it was reasonable to describe its structure by MRO model rather than CRN model [23].

Based on above literature survey, we know that the mechanism of SR in a-Ge is still in controversy, although much improvement has been made. In this paper, some experiments were conducted to shed some light on the debate between Cheng [16] and Roorda [17], and a general model for SR is proposed based on results of Theye's results with taking into account the existent of high volume of MRO. This model is appropriate for interpreting most of experimental and theoretical results.

© 2020 The Author(s). Published by IOP Publishing Ltd

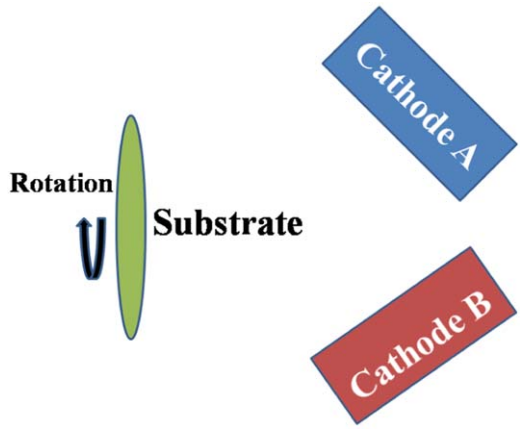

Figure 1. Sketch of our deposition system.

2. Experiment and method

a-Ge film was fabricated by a RF-MS deposition system ATC 2200-H (AJA Company, USA) in Ar (99.999%) gas. There are four sputtering sources in our deposition chamber, and they are configured in con-focal tilt mode, which is shown in figure 1. Two sources were used to deposit a-Ge film. The substrate was mounted between the two sources, and the distance between the substrate and sources is 80 mm. To obtain uniformity, the substrate is rotated at a speed of 40 rpm. Radio Frequency (Seren Company, USA) was used to deposit a-Ge. Ge (99.999%) target with a diameter of 4 inch was bought from Kurt J. Lesker Company. Radio Frequency was used to deposit a-Ge. The base pressure was 5×10^{-5} Pa, and the working pressure was 0.1 Pa. The sputtering power was kept at 200 W. a-Ge film was deposited on Φ30 mm fused silica substrate at room temperature. Film thickness was controlled only by deposition time. The deposition time for two kinds of samples is 5400 s and 7200 s, respectively.

Film thickness was measured by NEWVIEW 6000 interferometer (ZYGO Company, USA). Reflectance and transmission of thin films were characterized by Lambda 950 Spectrophotometer in the wavelength range of 500–2000 nm with a step of 1 nm, and the incident angle was fixed at 8 degree. Surface resistance was measured by JANDEL four point probing system (MODEL RM3-AR, 10 nA). It should mention that all surface resistance, reflectance and transmission measurements were performed at room temperature and ambient environment.

3. Result and discussion

It is well known that a-Ge film is easily oxidized when exposed to air, and the GeO_2 layer above a-Ge film is no more than 1.2 nm thick [24]. GeO_2 has a high resistivity of 0.1 MΩ·cm [25], while Ge 50 Ω·cm. Thus, GeO_2 layer has a negligible influence on surface resistance of a-Ge because GeO_2 layer and a-Ge film are connected in parallel with each other.

The optical band gap of amorphous materials can be obtained by Tauc's equation, which is given by [26–28]

$$(\alpha h\nu)^{1/n} = B(h\nu - E_g) \tag{1}$$

where $h\nu$ is the photon energy, B is the edge width parameter dependent on structural disorder of films, α is the absorption coefficient, and n is exponent. For Ge, known as an indirect semiconductor, n was chosen as 2 [26–28]. The absorption coefficient is characterized by $4\pi k/\lambda$, where k is extinction coefficient, and λ is wavelength. Extinction coefficient k can be determined by reflectance and transmission of thin films [29]. Figure 2 shows an Tauc plot of the sample with a thickness of 364.5 nm, the linear portion is extrapolated to yield the optical band gap E_g at $(\alpha h\nu)^{1/2} = 0$, and the value of E_g is 0.891 eV.

Table 1 shows results of surface resistance ρ_s and optical energy band gap E_g. Two samples were annealed at 300 °C in a vacuum chamber (3.0×10^{-5} Pa) after they were aged for two months. Surface resistance ρ_s and optical energy band gap E_g were characterized at different stages, such as as-deposited, aged, and annealed. The thickness of two samples is 364.5 and 486.0 nm, respectively. Surface resistance increased when samples underwent sequentially three stages. Band gap shows an increment of 0.011–0.013 eV at first-aged stage as compared to as-deposited stage, and 0.119–0.126 eV at annealed stage as compared to aged stage. An increment of 0.119–0.126 eV due to annealing shows good agreements with 0.12 [30] for a-Ge and 0.13 eV [31] for a-Si. It was proposed by Theye [4] that surface resistance increment after deposition was referred to as one

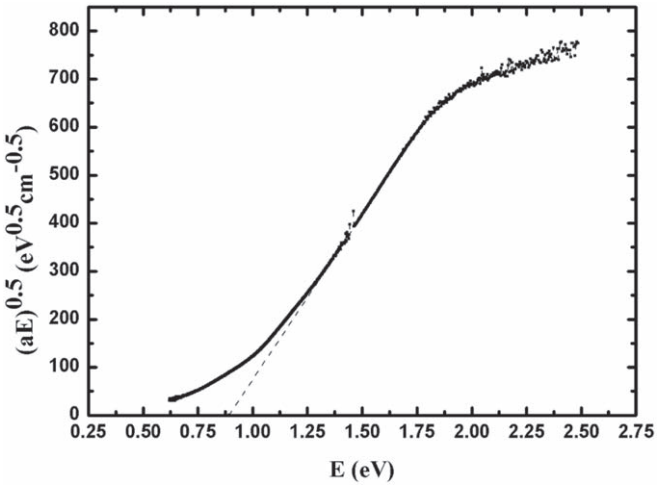

Figure 2. Tauc plot of the sample with a thickness of 364.5 nm.

Table 1. Results of surface resistance ρ_s and optical band gap E_g.

	SSR				AISR	
	As-deposited (i)		aged (ii) (two months)		Annealed (iii) (300 ± 5 °C)	
d^*	ρ_s^*	E_g^*	ρ_s	E_g	ρ_s	E_g
(nm)	(MΩ/□)	(eV)	(MΩ/□)	(eV)	(MΩ/□)	(eV)
364.5	3.05	0.891	4.54	0.904	14.30	1.023
486.0	2.82	0.884	4.07	0.895	10.80	1.021

*The error of surface resistance is ±1%, the error of band gap is ±0.02 eV, and the error of thickness is ±2.0 nm. Surface resistance of first sample was measured at 24.6, 21.6, and 20.9 °C, respectively. Surface resistance of second sample was measured at 22.0, 21.6, and 20.9 °C, respectively. The error of temperature is ±0.1 °C.

Table 2. Results of surface resistance ρ_s for samples kept at low temperature and room temperature, respectively.

	ρ_s^* (MΩ/□) (as-deposited)	Kept at temperature (°C)	ρ_s (MΩ/□) (after 7 days of SR)
#1	100.0	−195 ± 3	228.3
#2	99.5	23 ± 1	225.9

*The error of surface resistance is ±1%.

phenomenon of SSR. Here, besides surface resistance increment, an increment of 0.011–0.013 eV due to aging for two months is also shown in table 1, and this increment is another phenomenon of SSR. There are two reasons that this increment was not found out until now. Firstly, this increment is very small (only ~0.012 eV), and much care should be paid to measure it; secondly, as-deposited samples show fast SR, and they must be characterized as soon as possible.

3.1. SSR

3.1.1. SSR at low temperature

Two samples with a thickness of 100 nm were deposited simultaneously. One sample was kept at −195 °C in a vacuum chamber (10^{-5} Pa); the other one was kept at room temperature and ambient environment. After 7 days, two samples were simultaneously measured at room temperature and ambient environment. Table 2 shows results of surface resistance ρ_s for samples kept at low temperature and room temperature, respectively. They all show a similar resistivity increase; this implies that they all underwent SSR regardless of temperature. SSR can occur even though at very low temperature. This result informs us that SSR, different from AISR, does not need external activation energy.

Table 3. Experimental and theoretical simulated results of surface resistance ρ_s.

d^* (nm)	As-deposited (i)	Aged (ii) (two months)	
	Experiment (MΩ/□)	Experiment (MΩ/□)	Theory (MΩ/□)
364.5	3.05	4.54	5.08
486.0	2.82	4.07	4.35

Table 4. Experimental and theoretical results of decay time for SSR

	t_R	
d^* (nm)	Experiment* (hours)	Theory (hours)
364.5	9.0	8.9
486.0	7.0	6.5

*The error of experimental results about decay time of SSR is ±0.5 h.

3.1.2. Theoretical calculation of SSR

As shown in table 1, it is obvious that samples underwent SR after deposition. This process is spontaneous, and does not need external activation energy. The final surface resistance after spontaneous relaxation can be calculated by equation (2) [32–34].

$$R = R_0 \exp\left(\frac{\Delta E}{kT}\right) \tag{2}$$

where R_0 is initial surface resistance, ΔE is energy change, k is Boltzmann constant, and T is temperature. Here we regard band gap changes as energy changes. Table 3 shows experimental and theoretical simulated results of surface resistance after spontaneous relaxation. Theoretical results of surface resistance after spontaneous relaxation for 364.5, 486.0 nm samples are 5.08 and 4.35 MΩ/□, respectively, which shows good agreements with experimental results.

3.1.3. Time constant of SSR

Table 4 shows experimental and theoretical results of decay time for SSR. Theoretical results of decay time for SSR can be calculated by equation (3) [32].

$$R(t) = R_0\left(\frac{t_R}{t_0}\right)^{\nu} \tag{3}$$

where R_0 is initial surface resistance at initial time t_0, and ν is exponent factor. Samples were taken from deposition chamber after deposition, and they were characterized by surface resistance immediately. The time span between deposition ending and measurement is ten minutes, thus t_0 is ten minutes. ν is 0.1 according to [32]. Combined with experimental data in table 3, theoretical calculations were conducted. As shown in table 4, theoretical results (8.9 h of t_R for 364.5 nm sample, and 6.5 h for 486.0 nm sample) show good agreements with experimental ones (9.0 h of t_R for 364.5 nm sample, and 7.0 h for 486.0 nm sample).

3.2. AISR

As shown in figure 3, AISR process (1)–(2) can be divided into (1)–(3)–(4)–(2) steps. Band gap E_g is temperature dependence, which is calculated by Varshni equation (4) [35].

$$E_g(T) = E_g(0) - \frac{\alpha T^2}{T + \beta} \tag{4}$$

where $\alpha = 4.774 \times 10^{-4}$ eV/K, $\beta = 235$ K.

Surface resistance can be obtained by equation (5).

$$R = R^* \exp\left(\frac{E_a}{kT}\right) \tag{5}$$

where R^* is prefactor, E_a is activation energy for conduction, and k is Boltzmann constant. Here, E_a is a half of band gap [36]. Taken 364.5 nm sample as an example, AISR can be described in detail as below: (1) Initial state;

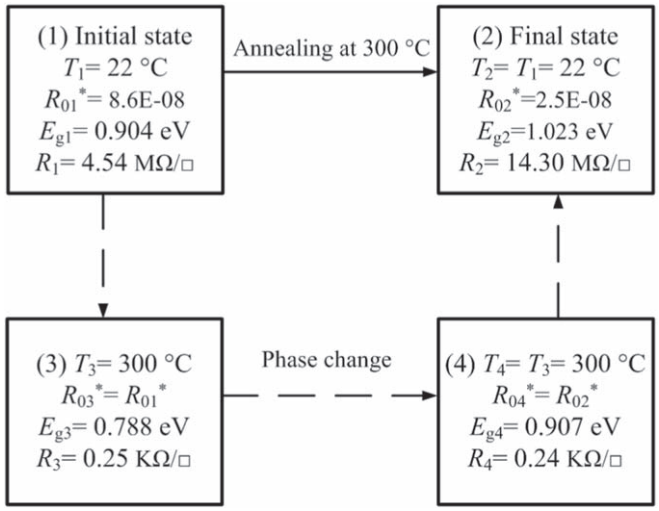

Figure 3. Scheme of AISR of 364.5 nm sample annealed at 300 °C.

(3) Annealing temperature increases to be 300 °C. Here, it is assuming that no phase change occurs in the process of temperature increasing from 22 to 300 °C. E_{g3} and R_3 can be obtained by equations (3) and (4), and R_{03}^* have the same value with R_{01}^*; (4) Due to phase change, R_{04}^* decreases from 8.6E08 to be 2.5E08 Ω/□, and E_{g4} increases from 0.788 to 0.907 eV. Surprisingly, surface resistance drops slightly. (2) Final state, temperature decreases from 300 to be 22 °C. R_{02}^* have the same value with R_{04}^*. Annealing alters band gap and R^*, finally, it results in an increase in band gap and surface resistance in State (2). However, surface resistance shows a slight decrease at 300 °C after annealing. Unfortunately, we have no equipment to *in situ* measure surface resistance at 300 °C, and cannot verify the correctness of this prediction.

It should be noted that CRN is dominant in our a-Ge films [37], SSR and AISR mentioned above in discussions about our samples all belong to CRN Sr.

3.3. MRO-to-CRN SR

We have no a-Ge films with high volume of MRO, so here we cite the results of Gibson group and Nakamura group. Gibson group employed fluctuation electron microscopy to characterize MRO in amorphous films, and they found that there is a reduction of MRO after thermal annealing. They pointed out that transformation from MRO to CRN occurs only at higher annealing temperature (larger than 500 °C for ion-implanted a-Si) [15, 16]. Nakamura group found that there was a structural transition from MRO to CRN due to aging at ambient temperature [20], electron irradiation [21], and thermal annealing [22], respectively. We believe that this is the third SR, referred to as MRO-to-CRN Sr.

4. Theory

In summary, figure 4 shows a general model for SR in a-Ge films. As shown in figure 4, when MRO is dominant in a-Ge films, some volumes of MRO will transform into CRN, and such a structure change is called MRO-to-CRN SR by us; when CRN is dominant, a-Ge films undergo SSR and AISr In addition, a-Ge films show an increase in band gap after three kinds of Sr This phenomenon due to SR can be interpreted by figure 5.

Figure 5 demonstrates the band gap structure of a-Ge (30, 31, 38, 40), which is cited from figure 9 of [30] and figure 8 of [31]. The shaded area represents the region of localized states, and optical band gap is equal to E_{g1} (E_{g2}) [30, 31, 38, 39]. It was reported that E_0 of high-quality CRN is 1.3 eV (0 K) [40]. Thus, the band gap can broaden to be larger than 1.3 eV. The CRN is not a unique structure, and CRN structures have different band gaps due to diverse strains and defects. The expansion of the band gap is relying on the quality of the CRN. Details about band gap change in a-Ge can be found in [39].

When MRO is dominant, the band gap narrows down as the strain is exerted on high volume fraction of topologically crystalline grains. There is a reduction in strain when there is a transition from MRO to CRN. Thus, band gap increases after MRO-to-CRN SR. Furthermore, surface resistance increases resulting from an increase in band gap [39].

When CRN is dominant, samples have CRN' structure with more defects and larger average bond-angle distortion, they have metastable state with high free energy. Through AISR, activation energy is exerted on a-Ge. Some defects and distortion reduce, and some defect states in LVB, LCB, and E_0 disappear. Correspondingly,

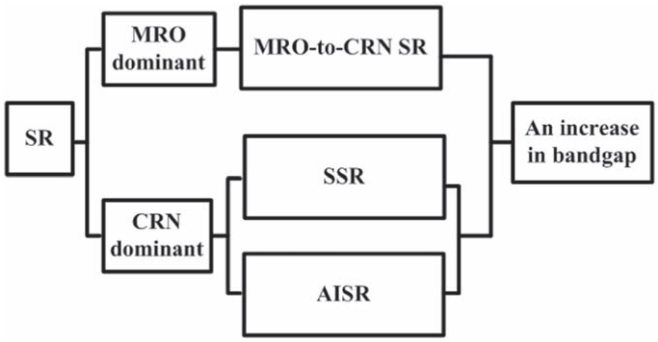

Figure 4. a general model for SR in a-Ge.

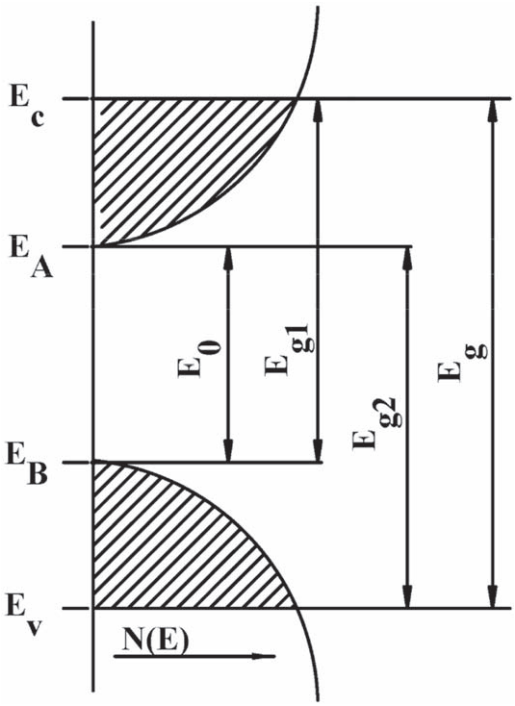

Figure 5. Mott-Davis model (see [30, 31, 38, 39]) of the density of states functions for a-Ge films.

band gap broadens. In other words, annealing is necessary if we want to obtain higher-quality CRN. Our phase change analysis in figure 3 indicates that there is a slight reduction in surface resistance at 300 °C after annealing (state 4 compares with state 3). Annealing results in band gap expansion and $R_0{}^*$ reduction, which alters temperature dependence of surface resistance, and finally leads to an increase in surface resistance (final state in figure 3). It should be noted that amorphous $Ge_2Sb_2Te_5$ films also show similar SR, and a similar mechanism is proposed to interpret SR [32].

The mechanism of AISR has been extensively studied by Roorda's group. They believe that AISR is a local structural change proceeding via the recombination of the dangling bands and the annihilation of point defects (vacancies and interstitials) [10]. Through this AISR, CRN' transforms into CRN with less defects and a reduction in average bond-angle distortion. It should be noted that annealing in AISR means that samples are kept at temperature higher than at which samples are prepared. Taken the research of Roorda' group as an example, a-Si was produced by ion implantation at liquid nitrogen temperature (−196 °C) in their experiment [8]. Thus, when a-Si was kept at −150 °C, it means that a-Si was annealing at −150 °C. Thus, AISR has a wide spectrum of activation energies because annealing can be performed at the temperature range from the temperature that sample was prepared to temperature prior to crystallization.

As-deposited a-Ge has a very thermodynamically unstable structure, and through SSR, a-Ge relaxes to a relatively stable state. SSR is structural inhomogeneity-driven relaxation process, it is a spontaneous atomic rearrangement [4], and this process does not need externally exerted activation energy.

Table 5. Lists of properties of SSR, AISR and MRO-to-CRN SR.

Parameter	SR		
	SSR	AISR	MRO-to-CRN SR
Temperature	independent	$>T_{PT}$ and $<T_{CT}$	$>T_S$
Activation energy	no	wide spectrum	higher
Time constant	several hours	107–443 S*	unknown
Mechanism	Inhomogeneity-driven	phase change	phase change
Bang gap	increase	increase	increase
Surface resistance	increase	decrease	increase

*This value is cited from [8].

Table 5 demonstrates the properties of SSR, AISR and MRO-to-CRN Sr T_{PT} is the temperature that sample was prepared, T_{CT} is crystallization temperature, and T_S is a higher specific temperature. From this summary, the difference among them is clear. However, there are still some unknown properties, such as time constant of MRO-to-CRN SR, mechanism of the increase of band gap and surface resistance for SSR, the factors that influence T_s of MRO-to-CRN Sr

5. Conclusions

SSR, AISR, and MRO-to-CRN SR all possibly occur in a-Ge films, and different structure determines that which one is dominant. When CRN is dominant, SSR and AISR (if samples are annealed) occur; when MRO is dominant, MRO-to-CRN SR occurs. In fact, SSR, AISR, and MRO-to-CRN SR often occur simultaneously, especially for MRO is dominant, but SSR and AISR contribute less to the whole Sr After undergoing three kinds of SR, samples all show band gap widening. The reason for an increase in band gap and surface resistance after SSR still needs further investigation. The prediction of an increase in band gap and surface resistance after MRO-to-CRN SR still needs experimental verification. Our work will attract much theoretical calculation for different SR and complicated SR mechanism, and some unknown properties of SR will be further understood.

Acknowledgments

This research is supported by the National Key R&D Program of China (No. 2017YFB0403802).

ORCID iDs

Ning-Ning Dong https://orcid.org/0000-0001-5707-5183
Xiaodong Wang https://orcid.org/0000-0001-6881-1211

References

[1] Deb S K, Wilding M, Somayazulu M and McMillan P F 2001 Pressure-induced amorphization and an amorphous-amorphous transition in densified porous silicon *Nature* **414** 528–30
[2] Vasisht V V, Saw S and Sastry S 2011 Liquid–liquid critical point in supercooled silicon *Nat. Phys.* **7** 549–53
[3] Hedler A, Klaumünzer S L and Wesch W 2004 Amorphous silicon exhibits a glass transition *Nat. Mater.* **3** 804–9
[4] Theye M L, Gheorghiu A, Gandais M and Fisson S 1980 Structural relaxation and crystallization of amorphous Ge films *J. Non-Cryst. Solids* **37** 301–23
[5] Tsu R, Hernandez J G and Pollak F H 1984 Determination of energy barrier for structural relaxation in a-Si and a-Ge by Raman Scattering *J. Non-Cryst. Solids* **66** 109–14
[6] Roorda S, Sinke W C, Poate J M, Jacobson D C, Dierker S, Dennis B S, Eaglesham D J, Spaepen F and Fuoss P 1991 Structural relaxation and defect annihilation in pure amorphous silicon *Phys. Rev. B* **44** 3702
[7] Roorda S, Doorn S, Sinke W C and Scholte P M L O and Loenen E van 1989 Calorimetric evidence for structural relaxation in amorphous silicon *Phys. Rev. Lett.* **62** 1880
[8] Roorda S 1999 Low temperature relaxation in amorphous silicon made by ion implantation *Nucl. Instrum. Methods Phys. Res. B* **148** 366

[9] Laaziri K, Kycia S, Roorda S, Chicoine M, Robertson J L, Wang J and Moss S C 1999 High resolution radial distribution function of pure amorphous silicon *Phys. Rev. Lett.* **82** 3460
[10] Urli X, Dias C L, Lewis L J and Roorda S 2008 Point defects in pure amorphous silicon and their role in structural relaxation: a tight-binding molecular-dynamics study *Phys. Rev. B* **77** 155204
[11] Roorda S, Martin C, Droui M, Chicoine M, Kazimirov A and Kycia S 2012 Disentangling neighbors and extended range density oscillations in monatomic amorphous semiconductors *Phys. Rev. Lett.* **108** 255501
[12] Treacy M M J, Gibson J M and Keblinski P J 1998 Paracrystallites found in evaporated amorphous tetrahedral semiconductors *J. Non-Cryst. Solids* **231** 99
[13] Treacy M M J and Borisenko K B 2012 The local structure of amorphous silicon *Science* **335** 950
[14] Gibson J M 2012 Solving amorphous structures-two pairs beat one *Science* **335** 929
[15] Gibson J M and Treacy M M J 1997 Diminished medium-range order observed in annealed amorphous germanium *Phys. Rev. Lett.* **78** 1074
[16] Cheng J-Y, Gibson J M, Baldo P M and Kestel B J 2002 Quantitative analysis of annealing-induced structure disordering in ion-implanted amorphous silicon *J. Vac. Sci. Technol. A* **20** 1855
[17] Roorda S 2003 Comment on 'quantitative analysis of annealing-induced structure disordering in ion-implanted amorphous silion *J. Vac. Sci. Technol. A* **21** 827
[18] Roorda S and Lewis L J 2012 Comment on 'The local structure of amorphous silicon *Science* **338** 1539
[19] Treacy M M J and Borisenko K B 2012 Response to comment on 'the local structure of amorphous silicon' *Science* **338** 1539
[20] Okugawa M, Nakamura R, Ishimaru M, Watanabe K, Yasuda H and Numakura H 2016 Structural transition in sputter-deposited amorphous germanium films by aging at ambient temperature *J. Appl. Phys.* **119** 214309
[21] Okugawa M, Nakamura R, Ishimaru M, Yasuda H and Numakura H 2016 Crystallization of sputter-deposited amorphous Ge films by electron irradiation: Effect of low-flux pre-irradiation *J. Appl. Phys.* **120** 134308
[22] Okugawa M, Nakamura R, Ishimaru M, Yasuda H and Numakura H 2016 Thermal crystallization of sputter-deposited amorphous Ge films: Competition of diamond cubic and hexagonal phases *AIP Adv.* **6** 125035
[23] Toh C *et al* 2020 Synthesis and properties of free-standing monolayer amorphous carbon *Nature* **577** 199
[24] Henrich V E and Fan J C C 1975 Auger spectroscopy studies of the oxidation of amorphous and crystalline germanium *J. Appl. Phys.* **46** 1206
[25] Krupanidhi S B and Sayer M 1984 Electrical characterization of amorphous germanium dioxide films *Thin Solid Films* **113** 173–84
[26] Demichelis F, Kaniadakis G, Tagliaferro A and Tresso E 1987 New approach to optical analysis of absorbing thin solid films *Appl. Opt.* **26** 1737
[27] Tsao C Y, Weber J W, Campbell P, Conibeer G, Song D and Green M A 2010 *In situ* low temperature growth of poly-crystalline germanium thin film on glass by RF magnetron sputtering *Sol. Energy Mater. Sol. Cells* **94** 1501–5
[28] Banerjee A N and Chattopadhyay K K 2005 Size-dependent optical properties of sputter-deposited nanocrystalline p-type transparent $CuAlO_2$ thin films *J. Appl. Phys.* **97** 084308
[29] Macleod H A 2010 *Thin-Film Optical Filters* (Boca Raton, FL: CRC Press)
[30] Tomlin S G, Khawaja E and Thutupalli G K M 1976 The optical properties of amorphous and crystalline germanium *J. Phys. C* **9** 4335
[31] Thutupalli G K M and Tomlin S G 1977 The optical properties of amorphous and crystalline silicon *J. Phys. C* **10** 467
[32] Fantini P, Brazzelli S, Cazzini E and Mani A 2012 Band gap widening with time induced by structural relaxation in amorphous $Ge_2Sb_2Te_5$ films *Appl. Phys. Lett.* **100** 013505
[33] Ielmini D and Zhang Y 2007 Analytical model for subthreshold conduction and threshold switching in chalcogenide-based memory devices *J. Appl. Phys.* **102** 054517
[34] Yelon A, Movaghar B and Branz H M 1992 Origin and consequences of the compensation (Meyer-Neldel) law *Phys. Rev. B* **46** 12244
[35] Varshni Y P 1967 Temperature dependence of the energy gap in semiconductors *Physica (Utrecht)* **34** 149
[36] Oosthoek J L M, Krebs D, Salinga M, Gravesteijn D J, Hurkx G A M and Kooi B J 2012 The influence of resistance drift on measurements of the activation energy of conduction for phase-change material in random access memory line cells *J. Appl. Phys.* **112** 084506
[37] Wang X D, Chen B, Wang H F, Chen B, Liu S J, Cui Z X, Li B, Wang J B, Wang S M and Li Y P 2015 Detection of medium-range-order structure in amorphous germanium films by spectroscopic ellipsometry *J. Appl. Cryst.* **48** 1011–5
[38] Mott N F 1993 *Conduction in Non-Crystalline Materials* (Oxford: Clarendon)
[39] Wang X D, Wang H F, Chen B, Li Y P and Ma Y Y 2013 A model for thickness effect on the band gap of amorphous germanium film *Appl. Phys. Lett.* **102** 202102
[40] Barkema G T and Mousseau N 2000High-quality continuous random networks *Phys. Rev. B* **62** 4985–90